



Domain wall motion in ferromagnetic nanostructures with a voltage-controlled gradient of perpendicular anisotropy and Dzyaloshinskii-Moriya interaction

Andrei I. Nikitchenko and Nikolay A. Pertsev *Department of Solid State Physics, Ioffe Institute, 194021 Saint Petersburg, Russia* (Received 26 June 2023; revised 8 November 2023; accepted 8 December 2023; published 26 December 2023)

Ferromagnet-dielectric nanostructures possessing voltage-controlled magnetic anisotropy provide valuable opportunities for the excitation and regulation of magnetization dynamics by an electric field created in the dielectric counterpart. Here, we theoretically investigate the electrically driven motion of 180° domain walls (DWs) in multilayer ferromagnetic nanotracks with a voltage-induced gradient of the perpendicular magnetic anisotropy (PMA) and the interfacial Dzyaloshinskii-Moriya interaction (DMI). Our paper includes micromagnetic simulations of the DW motion in the Pt/Co/MgO/Si and Pt/Fe/MgO/Si nanostructures and analytical calculations of the DW velocity in the frame of a collective coordinate model. It is shown that the PMA gradient created under the Si gate of a finite length L_{Si} gives rise to the DW movement over significant distances, which may strongly exceed L_{Si} in the presence of substantial DMI. Remarkably, the electrically driven DW motion over micrometer distances with the peak velocities up to 100 m/s can be achieved in the defect-free Pt/Fe/MgO/Si nanostructure. The numerical results are explained by the analytical model, which predicts that the DW velocity should rise with increasing PMA gradient and become higher in ferromagnets with a low magnetic damping. Similar predictions hold for the motion of the 180° DWs in antiferromagnetic nanostructures with the voltage-controlled PMA. Our findings provide guidelines for the development of energy-efficient spintronic devices employing mobile DWs.

DOI: [10.1103/PhysRevB.108.224432](https://doi.org/10.1103/PhysRevB.108.224432)

I. INTRODUCTION

Domain walls (DWs) in ferromagnets are topologically stable spin textures resulting from the rotation of the spontaneous magnetization. Mobile DWs can serve as information carriers in racetrack memories [1,2] and logic gates [3], while static DWs can be employed as reconfigurable magnonic waveguides [4,5]. The motion of DWs can be induced by various stimuli, such as external magnetic fields [6], spin-polarized electric currents [7–10], pure spin currents [11–13], and spin waves [14]. Currently, the studies of DW dynamics are mostly focused on ferromagnetic nanostructures, where DWs can be driven by the spin-transfer torque generated by a spin-polarized electric current or by the spin-orbit torque created by a spin current injected into the ferromagnet by an adjacent heavy metal.

In ferromagnetic heterostructures, however, the DW symmetry and mobility may be additionally affected by the presence of interfaces. In particular, the contact between a ferromagnet and a heavy metal usually gives rise to a substantial interfacial Dzyaloshinskii-Moriya interaction (DMI) stabilizing chiral Néel DWs [15,16]. Such walls can be efficiently driven by the current-induced spin-orbit torque in heavy-metal/ferromagnet heterostructures with a perpendicular magnetic anisotropy (PMA) [11,12]. Besides, very high velocities of the magnetic-field-driven DW motion can be obtained owing to the suppression of the Walker breakdown

by a strong DMI [17,18]. Interestingly, the application of a gate voltage to the Pt/Co/Pd structure leads to a substantial increase in the DW velocity, which was attributed to a slight modulation of the interfacial DMI [19].

To reduce the energy consumption of spintronic devices employing the DW motion, it is highly desirable to move and control DWs by an electric field rather than electric current or magnetic field. Such an opportunity appears in ferromagnet-dielectric nanostructures with a voltage-controlled magnetic anisotropy (VCMA), such as Fe/MgO, CoFeB/MgO, Co/MgO, and Co/SrTiO₃, where PMA of interfacial origin varies with the electric field created in the dielectric nanolayer [20–23]. Experimental studies already demonstrated that the VCMA effect enables one to control the velocity of the magnetic-field-driven DW motion by a voltage applied to the gate electrode [24–28]. It was also predicted theoretically that a gradient of PMA can significantly change the velocity of DW motion induced by the spin-orbit torque in the Ta/CoFe bilayer [29]. Furthermore, based on the results of micromagnetic simulations, some researchers claimed that the DW motion in a ferromagnet-dielectric nanostrip can be driven solely by the PMA gradient of sufficient magnitude [30,31]. However, no clear electric-field-induced DW motion was observed in the Ta/CoFe/MgO wire with the gate electrode having a spatially varying electrical potential [32].

In this paper, we theoretically study the DW motion occurring in ferromagnetic nanostructures, where a voltage-controlled PMA coexists with a substantial DMI. The structure comprises an ultrathin ferromagnetic stripe deposited on

*pertsev.domain@mail.ioffe.ru

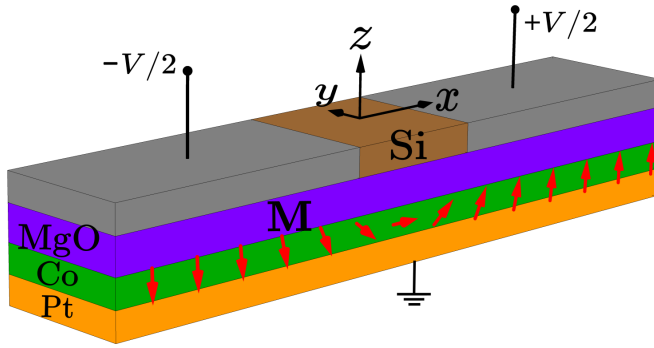


FIG. 1. Pt/Co/MgO trilayer bar with two metallic top electrodes separated by a Si gate. The voltages $-V/2$ and $+V/2$ applied to the electrodes generate an in-plane current in the Si gate, which creates a linearly varying electric field $E_z(x)$ in the underlying region of the MgO nanolayer. A grounded ultrathin Co layer with a perpendicular magnetic anisotropy contains a 180° DW.

a heavy metal inducing an interfacial DMI and covered by a dielectric nanolayer, which creates a PMA gradient regulated by a voltage applied to a semiconducting gate electrode (Fig. 1). We first carry out micromagnetic simulations of the voltage-induced DW dynamics in the Pt/Co/MgO/Si nanostructure and compare their results with those obtained for the Co/MgO/Si trilayer assumed to have no DMI. It is found that the PMA gradient gives rise to the DW motion in both nanostructures, but the DW movement over significant distances exceeding 100 nm occurs only in the presence of DMI. To clarify the mechanism of the voltage-induced DW motion, we then develop a simplified model based on the Lagrange formalism for the magnetization dynamics inside the wall, which enables us to derive an analytical relation for the DW velocity. This relation shows that the DW velocity depends on the deviation of the DW normal from the movement direction along the ferromagnetic stripe and on the orientation of the in-plane magnetization inside the wall (Fig. 2). Furthermore, the model predicts that the DW velocity could increase in ferromagnets with a low magnetic damping, which is confirmed by micromagnetic simulations performed for the Pt/Fe/MgO/Si nanostructure.

II. MICROMAGNETIC SIMULATIONS OF DOMAIN WALL MOTION

We study the motion of a 180° DW formed in an ultrathin Co stripe sandwiched between a Pt film and an MgO nanolayer covered by a metal top electrode with an inserted Si gate (Fig. 1). The thickness t_{Co} of the Co stripe is taken to be smaller than a critical thickness t_{SRT} , below which the perpendicular-to-plane orientation of the magnetization \mathbf{M} becomes stable in the Pt/Co/MgO structure. Since the estimated thickness $t_{\text{SRT}} \approx 2$ nm is much smaller than the exchange length $l_{\text{ex}} \approx 4.8$ nm of Co, a two-dimensional distribution $\mathbf{M}(x, y, t)$ of the dynamic magnetization is sufficient for the description of DW motion in the considered case. To determine this distribution under the assumption of constant saturation magnetization M_s , we carry out micromagnetic simulations with the aid of MUMAX3 software [33]. The torques involved in the Landau-Lifshitz-Gilbert

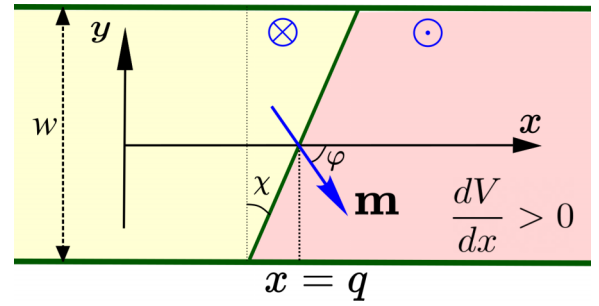


FIG. 2. Geometry of a 180° DW in an ultrathin ferromagnetic nanotrack with the width w . The angle χ quantifies the DW tilt from the plane orthogonal to the nanotrack axis x , and φ denotes the angle between the local in-plane magnetization inside DW and the axis x .

equation written for the unit vector $\mathbf{m} = \mathbf{M}/M_s$ are calculated by determining the total effective magnetic field $\mathbf{H}_{\text{eff}} = \mathbf{H}_{\text{ex}} + \mathbf{H}_{\text{dip}} + \mathbf{H}_{\text{an}} + \mathbf{H}_{\text{DMI}}$ acting on the magnetization, where \mathbf{H}_{ex} and \mathbf{H}_{dip} account for the exchange and dipolar interactions between spins in the Co stripe, \mathbf{H}_{an} is the contribution resulting from the magnetic anisotropy of the Pt/Co/MgO trilayer, and \mathbf{H}_{DMI} is the effective field caused by the interfacial DMI. The terms \mathbf{H}_{ex} and \mathbf{H}_{dip} are determined as described in Ref. [33], while the calculation of \mathbf{H}_{DMI} differs by the introduction of the factor D/t_{Co} , where D denotes the strength of interfacial DMI [34]. The field \mathbf{H}_{an} is the sum of the contributions originating from the cubic magnetocrystalline anisotropy of Co films [35] and the PMA created jointly by the Co/MgO and Pt/Co interfaces [36].

The PMA field \mathbf{H}_{PMA} has only one nonzero component H_z^{PMA} , which can be written in the first approximation as $H_z^{\text{PMA}} = -2(\mu_0 M_s t_{\text{Co}})^{-1} (K_s + K'_s) m_z$, where μ_0 is the magnetic permeability of free space, and K_s and K'_s are the parameters characterizing the magnetic anisotropy generated by the Co/MgO and Pt/Co interfaces, respectively [37]. When the top gate electrode has a nonzero electrostatic potential ϕ while the Co stripe is grounded, an electric field $E_z = -\phi/t_{\text{MgO}}$ appears in the MgO nanolayer with the thickness t_{MgO} , which changes the coefficient $K_s(E_z)$ associated with the Co/MgO interface [22,38]. In our case, the potential $\phi(x)$ varies linearly within the semiconducting gate, because the application of voltages $+V/2$ and $-V/2$ to the right and left metal pads creates direct electric current in Si (Fig. 1). Therefore, the electric field in the MgO nanolayer under the Si gate varies as $E_z = -\beta x/t_{\text{MgO}}$, where $\beta = V/L_{\text{Si}}$, and L_{Si} is the gate length. As a result, a voltage-controlled constant gradient of the PMA parameter K_s arises in the Co stripe. Since at the electric-field intensities up to 1 V nm^{-1} the dependence $K_s(E_z)$ is practically linear [38], the PMA field takes the form $H_z^{\text{PMA}} = -2(\mu_0 M_s t_{\text{Co}})^{-1} (K_s^\Sigma - k_s \beta x/t_{\text{MgO}}) m_z$, where $K_s^\Sigma = K_s(E_z = 0) + K'_s$, and $k_s = \partial K_s / \partial E_z$ is the electric-field sensitivity of K_s [39]. The effect of the electric field E_z in the MgO nanolayer on the DMI strength D is ignored in the simulations, because our analysis shows that the deviations $\delta D(E_z)$ from the zero-field value $D(E_z = 0)$ do not have any significant influence on the DW motion at the electric-field sensitivities $\partial D / \partial E_z < 70 \times 10^{-9} \text{ fJ V}^{-1}$ of the DMI strength in the Pt/Co/MgO and Pt/Fe/MgO nanostructures [40,41].

We perform simulations for the Co stripe with the length $L_{\text{Co}} = 2 \mu\text{m}$, width $w = 100 \text{ nm}$, and thickness $t_{\text{Co}} = 1.7 \text{ nm}$ assuming $t_{\text{MgO}} = 2 \text{ nm}$ and $L_{\text{Si}} = 200 \text{ nm}$. The stripe is modeled by a two-dimensional ensemble of computational cells with the in-plane dimensions $l_x = l_y = 2 \text{ nm}$ more than two times smaller than the exchange length of Co. The dynamics of the cell magnetizations are determined with the time step of 10 fs using the following set of material parameters: saturation magnetization $M_s = 1.45 \times 10^6 \text{ A m}^{-1}$ [42], exchange constant $A_{\text{ex}} = 30 \text{ pJ m}^{-1}$ [42], DMI strength $D = 2.17 \text{ pJ m}^{-1}$ [43], PMA parameter $K_s^\Sigma = -2.6 \text{ mJ m}^{-2}$ [36], VCMA sensitivity $k_s = -40 \text{ fJ V}^{-1} \text{ m}^{-1}$ [22], cubic-anisotropy coefficients $K_1 = 450 \text{ kJ m}^{-3}$ and $K_2 = 150 \text{ kJ m}^{-3}$ [44], and Gilbert damping parameter $\alpha = 0.03$ [45].

The simulations show that in the absence of PMA gradient the magnetization rotation across the introduced 180° DW occurs in the xz plane containing the normal to the Co stripe and its longitudinal axis. The polar angle θ of the magnetization vector $\mathbf{M}(x, y, t = 0)$ changes through the DW approximately as $\theta(x, y, t = 0) = 2\arctan[\exp(x/\lambda)]$, being almost the same along the stripe width w . Such a magnetization profile corresponds to the Néel DW with $m_x \partial m_z / \partial x > 0$ parallel to the yz plane. The effective DW width $\lambda \approx 10 \text{ nm}$ given by our numerical simulations is close to the theoretical value $\lambda = \sqrt{A_{\text{ex}} / (K_s^\Sigma t_{\text{Co}}^{-1} - N_z \mu_0 M_s^2 / 2)} \approx 12 \text{ nm}$ predicted for the 180° DW in the ultrathin Co nanotrack with the magnetic anisotropy dominated by the interfacial PMA and the demagnetizing factor $N_z = 0.967$ in the thickness direction [46].

When a PMA gradient is instantly created in the Co nanotrack, the DW begins to move away from its initial position $q(t = 0) = 0$ in the nanotrack center $x = 0$. Remarkably, the direction of the in-plane magnetization inside the moving DW gradually deflects from the x axis, which is accompanied by the deviation of the DW plane from the yz plane (see Fig. 2) without significant changes of the wall width λ measured along the normal to the wall plane. For the quantitative description of the DW motion, we use two coordinates: the average position $\langle q \rangle(t)$ of the DW center given by the relation

$$\langle q \rangle(t) = \frac{1}{w} \int_{-w/2}^{w/2} q(y, t) dy \quad (1)$$

and the average azimuthal angle $\langle \varphi \rangle(t)$ of the in-plane magnetization in the DW defined as

$$\langle \varphi \rangle(t) = \frac{1}{\lambda_\chi w} \int_{-w/2}^{w/2} \left[\int_{q(y,t)-\lambda_\chi/2}^{q(y,t)+\lambda_\chi/2} \varphi(x, y, t) dx \right] dy, \quad (2)$$

where $q(y, t)$ denotes the coordinate x at which $M_z(x, y, t) = 0$, $\lambda_\chi = \lambda / \cos \chi$, and χ is the time-dependent angle between the normal to the DW plane and the longitudinal axis x of the Co nanotrack. Figure 3 shows time dependences of the DW position $\langle q \rangle(t)$ and the azimuthal angle $\langle \varphi \rangle(t)$ predicted by the simulations performed for the Pt/Co/MgO/Si nanostructure at a representative value $\beta = 25 \text{ mV nm}^{-1}$ of the voltage gradient $\beta = V/L_{\text{Si}}$ controlling the PMA variation at the given MgO thickness. It can be seen that at first the DW accelerates rapidly and leaves the region beneath the Si gate in a short time of about 2 ns [Fig. 3(a)]. Then the DW velocity gradually decreases due to the absence of the driving force created by

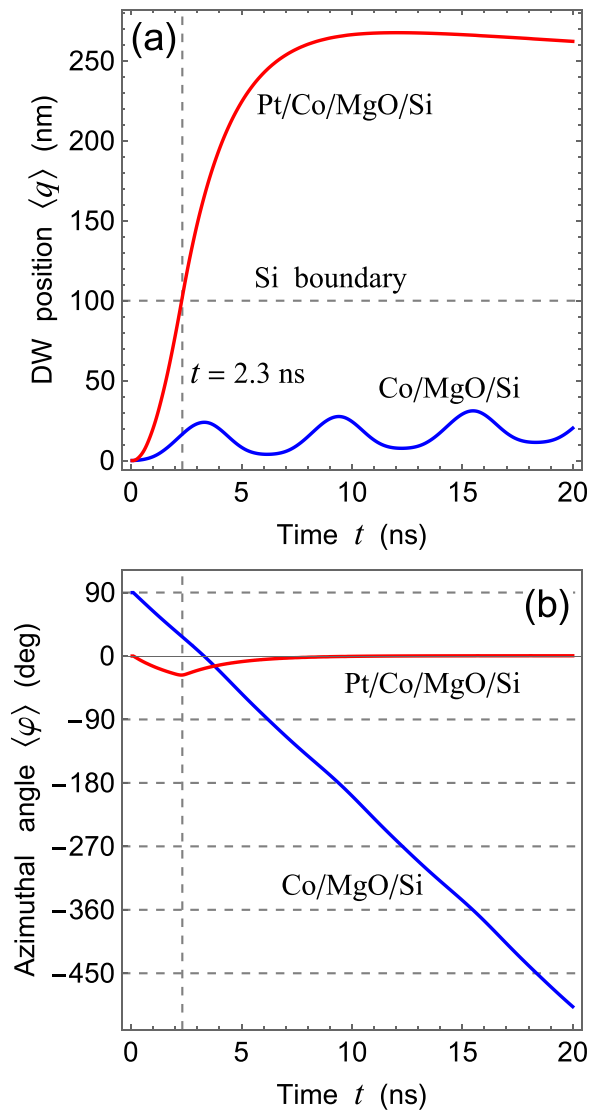


FIG. 3. Time dependences of (a) DW position $\langle q \rangle$ and (b) azimuthal angle $\langle \varphi \rangle$ of the in-plane magnetization in the DW calculated for the Pt/Co/MgO/Si and Co/MgO/Si nanostructures at the voltage gradient $\beta = 25 \text{ mV nm}^{-1}$. The vertical dashed line indicates the time $t = 2.3 \text{ ns}$, at which the DW in the Pt/Co/MgO/Si nanostructure passes under the boundary $x = 100 \text{ nm}$ of the Si gate.

the PMA gradient in this nanotrack region. At $t \approx 12 \text{ ns}$, the DW stops at a distance of about 260 nm from its initial position. Hereafter it moves back slowly under the action of effective force caused by the resulting reduction of the magnetostatic energy of the finite Co stripe. As demonstrated by Fig. 4, the maximal DW velocity and the largest DW displacement from the nanotrack center grow with increasing voltage parameter β controlling the PMA gradient.

To clarify the impact of DMI on the DW dynamics, we also perform simulations for the Co/MgO/Si trilayer having the same geometry and PMA gradient. Figure 3(a) shows that the DW motion in such a trilayer assumed to have no DMI differs drastically from the one revealed in the Pt/Co/MgO/Si nanostructure. Although the DW also moves away from the initial position, its voltage-induced motion

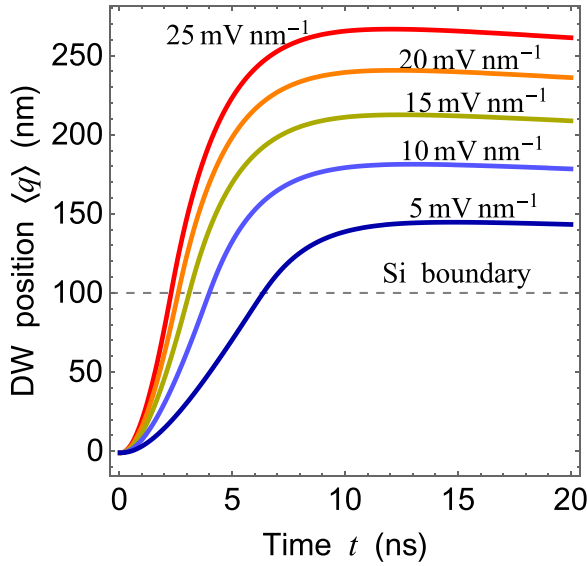


FIG. 4. Time dependences of the DW position $\langle q \rangle(t)$ in the Pt/Co/MgO/Si nanostructure calculated at different values of the voltage gradient β indicated on the plot.

has an oscillatory character, being limited to much smaller distances, which are less than 40 nm at $\beta = 25 \text{ mV nm}^{-1}$. Hence, we can conclude that the DMI strongly increases the displacements of DWs induced by the PMA gradient. This remarkable feature can be explained by very different evolutions of the average azimuthal angle $\langle \varphi \rangle(t)$ in the Néel wall appearing in the Pt/Co/MgO/Si nanostructure and the Bloch wall initially forming in the Co/MgO/Si trilayer [see Fig. 3(b)]. Interestingly, the DW moving in the Co/MgO/Si structure periodically transforms temporarily into the Néel wall ($\langle \varphi \rangle = 0, -180^\circ$), which results from continuous in-plane rotation of the magnetization inside the DW oriented orthogonally to the nanotrack axis ($\chi = 0$). A similar continuous rotation of the in-plane magnetization takes place when the Néel DW forms in an appropriate nanotrack having no DMI. Accordingly, this wall periodically transforms temporarily into the Bloch DW ($\langle \varphi \rangle = -90^\circ, -270^\circ$) so that the motion of initially different walls assumes the same character in the absence of DMI. Thus, the DMI stabilizes the time-dependent structure of the moving DW by preventing the transformation of the initial Néel-type wall into the Bloch one.

III. ANALYTICAL MODEL OF DOMAIN WALL MOTION

To derive an approximate analytical relation for the DW velocity, we construct a simplified model of the voltage-induced motion of the 180° DW in an ultrathin ferromagnetic nanotrack with an infinite length and a constant gradient dK_s/dx of the PMA parameter $K_s(x)$, which creates an effective field $H_z^{\text{grad}} = (\mu_0 M_s)^{-1} \lambda dK_s/dx$ acting on the DW [30]. The model describes the collective magnetization dynamics inside the moving DW with the aid of the Lagrangian approach [47], in which the azimuthal angle φ of the in-plane magnetization is assumed to be the same throughout the wall at each moment t . In accordance with the results of our micromagnetic simulations, the distribution of the polar angle θ in the moving DW may be approximated by the relation

$$\theta = 2 \arctan \left(\exp \left[\frac{x - q(t) + y \tan \chi(t)}{\lambda_\chi(t)} \right] \right), \quad (3)$$

where q denotes the position of the DW center in the nanotrack (see Fig. 2). Hence, the DW motion can be described by the collective coordinates $c_1 = q$, $c_2 = \varphi$, and $c_3 = \chi$. The Lagrange-Rayleigh equations then take the form ($i = 1, 2, 3$)

$$\frac{\partial L}{\partial c_i} - \frac{d}{dt} \left(\frac{\partial L}{\partial \dot{c}_i} \right) + \frac{\partial R}{\partial \dot{c}_i} = 0, \quad (4)$$

where $L(c_i, \dot{c}_i, t)$ is the Lagrange function and $R(c_i, \dot{c}_i, t)$ is the Rayleigh dissipation function. The functions involved in Eq. (4) should be evaluated by integrating their densities [48]

$$\begin{aligned} \frac{dL}{dx dy dz} &= F + \frac{M_s}{\gamma} \varphi \dot{\theta} \sin \theta, \\ \frac{dR}{dx dy dz} &= \frac{\alpha M_s}{2\gamma} [(\dot{\theta})^2 + (\dot{\varphi})^2 \sin^2 \theta] \end{aligned} \quad (5)$$

over the volume of the ferromagnetic nanotrack. In Eq. (5) γ is the gyromagnetic ratio, and $F = F_{\text{ex}} + F_{\text{dip}} + F_{\text{an}} + F_{\text{DMI}}$ is the micromagnetic energy density comprising the contributions resulting from the exchange and dipolar interactions, crystalline and interfacial magnetic anisotropies of the nanotrack, and interfacial DMI [34]. Differentiating Eqs. (3) and (5) and integrating over the volume of an infinitely long nanotrack, one can derive analytical relations for the derivatives involved in Eq. (4). The substitution of these relations into Eq. (4) and appropriate mathematical manipulation leads to the following system of differential equations for the collective coordinates:

$$\begin{aligned} \dot{q} &= \frac{\gamma}{(1 - \alpha^2) \cos \chi} \left[\frac{\alpha \lambda^2}{M_s \cos \chi} \tilde{k}_s + \frac{\pi D \sin(\varphi - \chi)}{2M_s t_F} - \frac{\lambda}{2} \mu_0 H_{\text{DW}} \sin[2(\varphi - \chi)] \right], \\ \dot{\varphi} &= \frac{\gamma}{1 - \alpha^2} \left[\frac{\lambda}{M_s \cos \chi} \tilde{k}_s - \frac{\pi \alpha D \sin(\varphi - \chi)}{2M_s \lambda t_F} + \frac{\alpha}{2} \mu_0 H_{\text{DW}} \sin[2(\varphi - \chi)] \right], \\ \dot{\chi} &= \frac{6\gamma}{\alpha t_F w^2} \left\{ \pi \lambda \frac{D \sin \varphi}{M_s \cos \chi} - \mu_0 H_{\text{DW}} \lambda^2 t_F \sin[2(\varphi - \chi)] \right. \\ &\quad \left. - \left[\frac{2A_{\text{ex}}}{M_s} t_F + \lambda^2 \left(\frac{2K_s}{M_s} - \mu_0 M_s t_F N_z \right) + \mu_0 H_{\text{DW}} \lambda^2 t_F \cos^2(\varphi - \chi) \right] \tan \chi \right\}, \end{aligned} \quad (6)$$

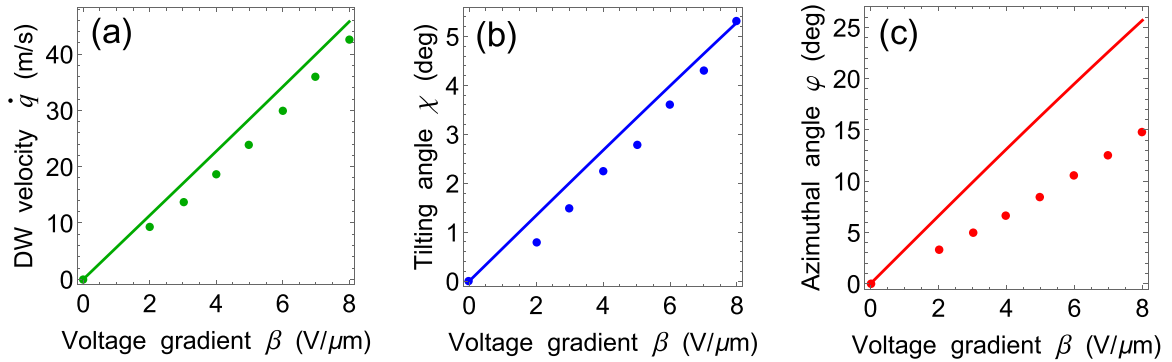


FIG. 5. Dependences of (a) DW velocity \dot{q} , (b) DW tilting angle χ , and (c) azimuthal angle φ of the in-plane magnetization in the DW on the voltage gradient β predicted for the Pt/Co/MgO/Si nanostructure by the collective coordinate model (lines) in comparison with the results of micromagnetic simulations (dots).

where $\tilde{k}_s = t_F^{-1} \partial K_s / \partial x$, t_F and w denote the nanotrack thickness and width, and $H_{\text{DW}} = \ln(2) M_s t_F / (\pi \lambda)$ is the magnitude of the mean demagnetizing field projection on the normal of the DW plane [49].

The inspection of Eq. (6) reveals that the initial movement of the Néel DW under the gate is driven only by the gradient dK_s/dx of the PMA parameter (as $\varphi = \chi = 0$ at $t = 0$). However, the PMA gradient also initiates the rotation of the in-plane magnetization inside the wall away from its original orientation along the nanotrack axis ($\dot{\varphi} \neq 0$ because of the term proportional to \tilde{k}_s). As a result, the azimuthal angle φ increases with time, which is accompanied by a tilt $\chi < \varphi$ of the DW plane. The terms depending on the difference $\varphi - \chi$ come into play, and the DW velocity \dot{q} increases strongly in the presence of significant DMI [see Fig. 3(a)]. Furthermore, it can be inferred that the wall should continue its motion even outside the region of the PMA gradient, where $\tilde{k}_s = 0$, because \dot{q} remains nonzero due to the term proportional to the DMI parameter D . Such a DMI-induced wall motion continues until the tilted DW configuration relaxes back to the initial nontilted one with $\varphi = \chi = 0$. This specific DW motion is driven by the magnetization precession around the normal to the wall plane, which provides the relaxation of the excess energy of the tilted DW that originates from the DMI. Thus, the predicted movement of the Néel DW outside the region of the PMA gradient should be regarded as a relaxation process. Since it occurs in the absence of any external force acting on the ferromagnetic heterostructure, it can be considered as a kind of inertial motion as well [50].

Interestingly, the equation obtained for the derivative $\dot{\varphi}$ is similar to Adler's equation [51], which has different types of solution depending on the ratio of two coefficients involved in its right-hand side. Therefore, the stationary solution $\dot{\varphi} = \dot{\chi} = 0$ of Eq. (6) exists only when the DMI strength is higher than some threshold value $D^*(\tilde{k}_s)$, whereas at $D < D^*(\tilde{k}_s)$ the angle φ experiences unlimited growth. Since the DW velocity \dot{q} depends on the sine functions of $\varphi - \chi$, at $D < D^*(\tilde{k}_s)$ the DW should exhibit an oscillatory motion similar to that shown in Fig. 3(a) for the Co/MgO/Si nanostructure. In contrast, the DW movement with the constant velocity \dot{q} depending on the stationary values of φ and χ becomes possible at $D > D^*(\tilde{k}_s)$.

For the steady-state DW motion, the numerical solution of Eq. (6) makes it possible to determine values of the DW

velocity \dot{q} and the stationary angles φ and χ at a given set of the involved parameters of ferromagnetic heterostructure. The results obtained for the Pt/Co/MgO/Si nanostructure ($\tilde{k}_s = k_s \beta t_{\text{MgO}}^{-1} t_{\text{Co}}^{-1}$) are presented in Fig. 5 together with the data extracted from our micromagnetic simulations. It can be seen that the collective coordinate model (CCM) describes the dependence of the DW velocity on the voltage gradient β with a good accuracy [Fig. 5(a)]. The variation of the DW tilting angle χ with β also agrees with the results of micromagnetic simulations [Fig. 5(b)]. However, the CCM overestimates the azimuthal angle φ by almost two times [Fig. 5(c)], which may be attributed to the assumption of its constancy across the DW region. This statement is confirmed by the analysis of our simulation data obtained for the Pt/Co/MgO/Si structure, which demonstrates rather large variations of the angle φ inside the moving DW.

Since the analytical calculations provide a reasonable description of the DW motion driven by the voltage gradient, we can use the CCM to reveal some important features of such motion. To that end, we linearize Eq. (6) with respect to the angles φ and χ and solve the linearized system of equations at $D > D^*(\tilde{k}_s)$ in the steady-state case. The obtained solution shows that at $\varphi, \chi \ll 1$ and $\alpha \ll 1$ the DW velocity is given by the relation

$$\dot{q} \approx -\frac{\gamma \lambda^2 \tilde{k}_s}{\alpha M_s}. \quad (7)$$

Equation (7) demonstrates that the DW velocity should be directly proportional to the PMA gradient \tilde{k}_s and inversely proportional to the Gilbert damping parameter α in the considered situation. Besides, the steady-state velocity appears to be independent of the DMI strength D , which, however, governs the distortion $\varphi - \chi \approx 2\lambda^2 \tilde{k}_s / [\alpha (2\mu_0 H_{\text{DW}} M_s \lambda - \pi D t_F^{-1})]$ of the moving Néel wall.

Importantly, the CCM model predicts that a low magnetic damping is favorable for the fast motion of the 180° Néel DWs induced by the PMA gradient. This feature can be explained by considering various torques appearing in the Landau-Lifshitz-Gilbert equation for the magnetization dynamics in the DW. When the PMA gradient is created in the ferromagnetic film, the Néel DW starts to move relatively slowly towards the region with a weaker PMA. This motion is accompanied by the magnetization precession, which leads

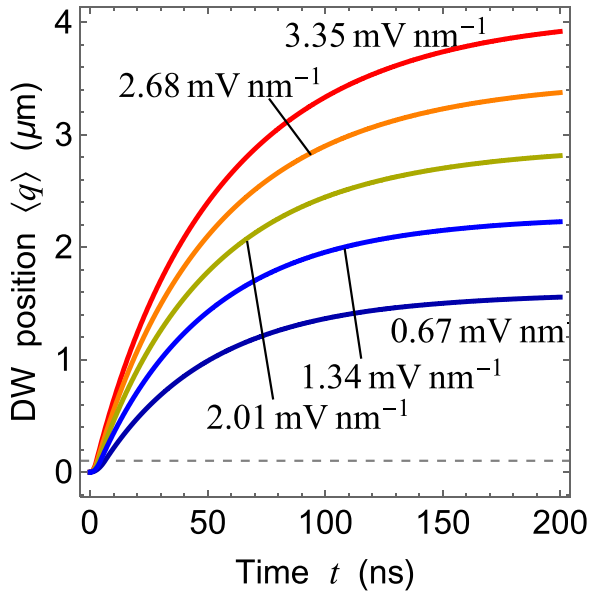


FIG. 6. Time dependences of the DW position $\langle q \rangle(t)$ in the Pt/Fe/MgO/Si nanostructure calculated at different values of the voltage gradient β indicated on the plot. These values provide the same PMA gradients as in the Pt/Co/MgO/Si nanostructure subjected to the voltage gradients β specified in Fig. 4. The Fe nanotrack has the length of $30 \mu\text{m}$, the length of the Si gate amounts to 200 nm , and the MgO thickness equals 2 nm .

to the appearance of nonzero angle $\varphi - \chi$ between the in-plane magnetization in the DW and the DMI field \mathbf{H}_{DMI} . The angle $\varphi - \chi$ governs the DMI torques $-\gamma\mu_0\mathbf{m} \times \mathbf{H}_{\text{DMI}}$ and $-\alpha\gamma\mu_0\mathbf{m} \times (\mathbf{m} \times \mathbf{H}_{\text{DMI}})$ involved in the Landau-Lifshitz-Gilbert equation, the first of which strongly accelerates the DW motion, whereas the second impedes this motion. Since the latter “damping” torque is proportional to the Gilbert parameter α , the Néel DWs could move faster in ferromagnets with a low magnetic damping.

To check this prediction, we perform micromagnetic simulations of the voltage-induced DW motion in the Pt/Fe/MgO/Si nanostructure, which differs from the Pt/Co/MgO/Si one by much smaller Gilbert parameter $\alpha = 0.0025$ of Fe [52]. For the Fe nanolayer, we use the following set of material parameters: $M_s = 1.71 \times 10^6 \text{ A m}^{-1}$ [53], $A_{\text{ex}} = 20 \text{ pJ m}^{-1}$ [54], $D = 1.02 \text{ pJ m}^{-1}$ [41], $K'_s = -0.23 \text{ mJ m}^{-2}$ [55], $K_s(E_z = 0) = -0.9 \text{ mJ m}^{-2}$ [53], $k_s = -100 \text{ fJ V}^{-1} \text{ m}^{-1}$ [20], $K_1 = 48 \text{ kJ m}^{-3}$ [54], and $K_2 = 15 \text{ kJ m}^{-3}$ [42]. The width $w = 100 \text{ nm}$ of the Fe nanotrack coincides with that of the Co one, but the Fe thickness is set to 0.57 nm to ensure the same theoretical DW width $\lambda \approx 12 \text{ nm}$ in the Co and Fe nanolayers. The results of simulations are presented in Fig. 6, which shows time dependences of the DW position $\langle q \rangle(t)$ in the Fe nanotrack at different values of the voltage gradient $\beta = V/L_{\text{Si}}$. Remarkably, the PMA gradient acting on the path $L_{\text{Si}}/2$ of only 100 nm provides the long-range DW movement over several micrometers. Despite two times smaller DMI strength, the maximal DW velocity in the Fe nanotrack appears to be much higher than that in the Co nanotrack at the same PMA gradient (e.g., 85 m/s vs 25 m/s at $\tilde{k}_s = -2.9 \times 10^{11} \text{ J m}^{-4}$). Furthermore, at $L_{\text{Si}} = 240 \text{ nm}$ even velocities up to 100 m/s

can be reached in the Fe nanotrack, where DW moves over distances $q \geq 5 \mu\text{m}$. Thus, the micromagnetic simulations demonstrate that the Pt/Fe/MgO/Si nanostructure is more suitable for the realization of voltage-driven DW motion than the Pt/Co/MgO/Si one.

It should be noted that our theoretical predictions are directly applicable only to defect-free ferromagnetic nanotracks. Indeed, it is well known that the interaction of DWs with various defects existing in ferromagnetic films usually has a strong influence on the DW motion, which takes the form of a thermally activated creep at low driving stimuli [56]. However, the DW dynamics may become very different in high-quality nanowires with a weak pinning. For example, fast DW motion with the velocities up to 80 m/s occurring over long distances $\sim 5 \mu\text{m}$ is observed in the permalloy nanowire under weak magnetic fields of a few oersted [57]. Importantly, the DW velocity is found to be proportional to the field intensity, and the DW mobility is close to the theoretical mobility $\mu_{\text{DW}} = \gamma\lambda/\alpha$ determined by the Gilbert damping parameter α [57]. Hence, the predicted long-range DW motion induced by the PMA gradient could be realized in high-quality nanotracks with a weak pinning.

Finally, we note that the voltage-controlled interfacial magnetic anisotropy should exist in antiferromagnet-dielectric bilayers as well [58]. Therefore, the DW motion driven by the voltage-induced PMA gradient, which was proposed recently [59], could be realized in suitable antiferromagnetic heterostructures. Motivated by this opportunity, we carried out micromagnetic simulations of the effect of DMI on the motion of 180° Néel DWs in an ultrathin antiferromagnetic film with the voltage-controlled PMA gradient created as described in Fig. 1 and an interfacial DMI. The simulations of the spin dynamics in a model two-sublattice antiferromagnet demonstrate that the maximal DW velocity reached inside the region of the PMA gradient may exceed 1 km/s at the Gilbert damping parameter $\alpha < 10^{-3}$. Interestingly, the DW velocity appears to be almost insensitive to the presence of DMI, because its influence is suppressed by the antiferromagnetic exchange. Nevertheless, the DW movement beyond the gate electrode should be possible in antiferromagnets with a low damping parameter $\alpha < 10^{-3}$. Thus, both ferromagnetic and antiferromagnetic nanoheterostructures possessing the voltage-controlled PMA could be suitable for the realization of the electrically driven long-range DW motion.

IV. CONCLUSION

In this paper, we presented theoretical results for the electrically driven motion of 180° DWs in ferromagnetic nanotracks with the PMA gradient created under the semi-conducting gate electrode and the DMI of interfacial origin. Micromagnetic simulations performed for the Co/MgO/Si and Pt/Co/MgO/Si nanostructures enabled us to reveal the influence of DMI on the DW motion induced by the in-plane voltage gradient β in the Si gate, which modifies the PMA associated with the Co/MgO interface. It was found that the Bloch DW, which forms in the Co/MgO/Si trilayer assumed to have no DMI, experiences comparatively slow motion of oscillatory character, which is limited to distances much smaller than the gate length $L_{\text{Si}} = 200 \text{ nm}$. In contrast,

the Néel DW appearing in the Pt/Co/MgO/Si nanostructure rapidly moves away from the region beneath the Si gate and may shift from its initial position by more than 250 nm, which demonstrates strong increase in the voltage-driven DW movement in the presence of substantial DMI.

Introducing collective coordinates and using the Lagrangian approach, we also developed an analytical model of the DW motion in an infinite ferromagnetic nanotrack with a linearly varying PMA strength. This collective coordinate model yielded a system of equations, which relates the DW velocity \dot{q} to the azimuthal angle φ of the in-plane magnetization inside the wall and the DW tilting angle χ and determines the steady-state values of \dot{q} , φ , and χ for nanotracks with sufficiently strong DMI. The calculations showed that, at φ , $\chi \ll 1$, the steady-state DW velocity is directly proportional to the gradient of the PMA strength and inversely proportional to the Gilbert damping parameter. In this range of φ and χ , \dot{q} is also independent of the DMI strength D , but it weakly grows with increasing D when the angles φ and χ become significant.

Since the analytical model predicts that the Néel DWs could move faster in ferromagnets with a low magnetic damping, we also performed micromagnetic simulations of the voltage-induced DW motion in the Pt/Fe/MgO/Si nanostructure, which differs from the Pt/Co/MgO/Si one by much smaller Gilbert parameter α . It was found that the voltage gradient of only 3.35 mV nm^{-1} gives rise to the DW movement over $5 \text{ }\mu\text{m}$ in the Fe nanotrack, during which the maximal wall velocity reaches 100 m/s . Remarkably, such a long-range

motion is initiated by the localized PMA gradient acting on the DW along a short path of only 120 nm . The subsequent “inertial” DW movement in the absence of any external stimulus can be explained by a slow relaxation of the tilted DW configuration, which is caused by the combined action of the PMA gradient and DMI under the gate electrode.

Thus, our theoretical results show that the ferromagnetic and antiferromagnetic nanoheterostructures possessing the voltage-controlled PMA are very promising for the development of efficient DW devices. Indeed, the excitation of the DW motion by an electric-field gradient created in the dielectric nanolayer should greatly reduce the power consumption in comparison with alternative devices driven by magnetic fields or spin-polarized currents. Furthermore, the presence of DMI or antiferromagnetic exchange ensures the long-range DW propagation with rather high velocities, which does not require the creation of the PMA gradient in the whole nanotrack. These features are important for the successful implementation of information-processing DW devices such as racetrack memories [1,2] and logic gates [3].

ACKNOWLEDGMENTS

We acknowledge financial support from the Russian Science Foundation (Project No. 23-12-00251 [60]) provided for the study of electrically induced spin dynamics in antiferromagnetic nanostructures.

-
- [1] S. S. P. Parkin, M. Hayashi, and L. Thomas, Magnetic domain-wall racetrack memory, *Science* **320**, 190 (2008).
 - [2] S. Parkin and S. Yang, Memory on the racetrack, *Nat. Nanotechnol.* **10**, 195 (2015).
 - [3] Z. Luo, A. Hrabec, T. P. Dao, G. Sala, S. Finizio, J. Feng, S. Mayr, J. Raabe, P. Gambardella, and L. J. Heyderman, Current-driven magnetic domain-wall logic, *Nature (London)* **579**, 214 (2020).
 - [4] F. Garcia-Sanchez, P. Borys, R. Soucaille, J.-P. Adam, R. L. Stamps, and J.-V. Kim, Narrow magnonic waveguides based on domain walls, *Phys. Rev. Lett.* **114**, 247206 (2015).
 - [5] K. Wagner, A. Kákay, K. Schultheiss, T. Henschke, A. Sebastian, and H. Schultheiss, Magnetic domain walls as reconfigurable spin-wave nanochannels, *Nat. Nanotechnol.* **11**, 432 (2016).
 - [6] F. H. D. Leeuw, R. V. D. Doel, and U. Enz, Dynamic properties of magnetic domain walls and magnetic bubbles, *Rep. Prog. Phys.* **43**, 689 (1980).
 - [7] J. Grollier, A. Chanthbouala, R. Matsumoto, A. Anane, V. Cros, F. Nguyen van Dau, and A. Fert, Magnetic domain wall motion by spin transfer, *C. R. Phys.* **12**, 309 (2011).
 - [8] J. Shibata, G. Tatara, and H. Kohno, A brief review of field- and current-driven domain-wall motion, *J. Phys. D* **44**, 384004 (2011).
 - [9] Z. Z. Sun, J. Schliemann, P. Yan, and X. R. Wang, Current-induced domain wall motion with adiabatic and nonadiabatic spin torques in magnetic nanowires, *Eur. Phys. J. B* **79**, 449 (2011).
 - [10] K.-J. Kim, R. Hiramatsu, T. Koyama, K. Ueda, Y. Yoshimura, D. Chiba, K. Kobayashi, Y. Nakatani, S. Fukami, M. Yamanouchi, H. Ohno, H. Kohno, G. Tatara, and T. Ono, Two-barrier stability that allows low-power operation in current-induced domain-wall motion, *Nat. Commun.* **4**, 2011 (2013).
 - [11] S. Emori, U. Bauer, S.-M. Ahn, E. Martinez, and G. S. D. Beach, Current-driven dynamics of chiral ferromagnetic domain walls, *Nat. Mater.* **12**, 611 (2013).
 - [12] K.-S. Ryu, L. Thomas, S.-H. Yang, and S. Parkin, Chiral spin torque at magnetic domain walls, *Nat. Nanotechnol.* **8**, 527 (2013).
 - [13] J. Lu and X. R. Wang, Motion of transverse domain walls in thin magnetic nanostripes under transverse magnetic fields, *J. Appl. Phys.* **107**, 083915 (2010).
 - [14] X.-g. Wang, G.-h. Guo, Y.-z. Nie, G.-f. Zhang, and Z.-x. Li, Domain wall motion induced by the magnonic spin current, *Phys. Rev. B* **86**, 054445 (2012).
 - [15] M. Heide, G. Bihlmayer, and S. Blügel, Dzyaloshinskii-Moriya interaction accounting for the orientation of magnetic domains in ultrathin films: Fe/W(110), *Phys. Rev. B* **78**, 140403(R) (2008).
 - [16] A. Thiaville, S. Rohart, É. Jué, V. Cros, and A. Fert, Dynamics of Dzyaloshinskii domain walls in ultrathin magnetic films, *Europhys. Lett.* **100**, 57002 (2012).
 - [17] Y. Yoshimura, K.-J. Kim, T. Taniguchi, T. Tono, K. Ueda, R. Hiramatsu, T. Moriyama, K. Yamada, Y. Nakatani, and T. Ono, Soliton-like magnetic domain wall motion induced by the

- interfacial Dzyaloshinskii–Moriya interaction, *Nat. Phys.* **12**, 157 (2016).
- [18] T. H. Pham, J. Vogel, J. Sampaio, M. Vaňatka, J.-C. Rojas-Sánchez, M. Bonfim, D. S. Chaves, F. Choueikani, P. Ohresser, E. Otero, A. Thiaville, and S. Pizzini, Very large domain wall velocities in Pt/Co/GdOx and Pt/Co/Gd trilayers with Dzyaloshinskii-Moriya interaction, *Europhys. Lett.* **113**, 67001 (2016).
- [19] T. Koyama, Y. Nakatani, J. Ieda, and D. Chiba, Electric field control of magnetic domain wall motion via modulation of the Dzyaloshinskii-Moriya interaction, *Sci. Adv.* **4**, eaav0265 (2018).
- [20] T. Nozaki, A. Koziol-Rachwał, W. Skowroński, V. Zayets, Y. Shiota, S. Tamaru, H. Kubota, A. Fukushima, S. Yuasa, and Y. Suzuki, Large voltage-induced changes in the perpendicular magnetic anisotropy of an MgO-based tunnel junction with an ultrathin Fe layer, *Phys. Rev. Appl.* **5**, 044006 (2016).
- [21] J. G. Alzate, P. Khalili Amiri, G. Yu, P. Upadhyaya, J. A. Katine, J. Langer, B. Ocker, I. N. Krivorotov, and K. L. Wang, Temperature dependence of the voltage-controlled perpendicular anisotropy in nanoscale MgO-CoFeB-Ta magnetic tunnel junctions, *Appl. Phys. Lett.* **104**, 112410 (2014).
- [22] H. Nakayama, T. Nozaki, T. Nozaki, and S. Yuasa, Engineering Co/MgO interface with heavy metals for voltage-controlled magnetic anisotropy effect, *Appl. Phys. Lett.* **122**, 032403 (2023).
- [23] B. F. Vermeulen, J. Swerts, S. Couet, M. Popovici, I. P. Radu, J. Van de Vondel, K. Temst, G. Groeseneken, and K. Martens, Electronic voltage control of magnetic anisotropy at room temperature in high- κ SrTiO₃/Co/Pt trilayer, *Phys. Rev. Mater.* **4**, 114415 (2020).
- [24] A. Schellekens, A. van den Brink, J. Franken, H. Swagten, and B. Koopmans, Electric-field control of domain wall motion in perpendicularly magnetized materials, *Nat. Commun.* **3**, 847 (2012).
- [25] U. Bauer, S. Emori, and G. S. D. Beach, Electric field control of domain wall propagation in Pt/Co/GdOx films, *Appl. Phys. Lett.* **100**, 192408 (2012).
- [26] D. Chiba, M. Kawaguchi, S. Fukami, N. Ishiwata, K. Shimamura, K. Kobayashi, and T. Ono, Electric-field control of magnetic domain-wall velocity in ultrathin cobalt with perpendicular magnetization, *Nat. Commun.* **3**, 888 (2012).
- [27] H. Kakizakai, K. Yamada, M. Kawaguchi, K. Shimamura, S. Fukami, N. Ishiwata, D. Chiba, and T. Ono, Direct observation of domain wall motion in Co/Pt wire under gate electric field, *Jpn. J. Appl. Phys.* **52**, 070206 (2013).
- [28] W. Lin, N. Vernier, G. Agnus, K. Garcia, B. Ocker, W. Zhao, E. E. Fullerton, and D. Ravelosona, Universal domain wall dynamics under electric field in Ta/CoFeB/MgO devices with perpendicular anisotropy, *Nat. Commun.* **7**, 13532 (2016).
- [29] Y. Zhang, S. Luo, X. Yang, and C. Yang, Spin-orbit-torque-induced magnetic domain wall motion in Ta/CoFe nanowires with sloped perpendicular magnetic anisotropy, *Sci. Rep.* **7**, 2047 (2017).
- [30] K. Yamada, S. Murayama, and Y. Nakatani, Magnetic domain wall motion in Co/Ni nanowires induced by a sloped electric field, *Appl. Phys. Lett.* **108**, 202405 (2016).
- [31] F. N. Tan, W. L. Gan, C. C. I. Ang, G. D. H. Wong, H. X. Liu, F. Poh, and W. S. Lew, High velocity domain wall propagation using voltage controlled magnetic anisotropy, *Sci. Rep.* **9**, 7369 (2019).
- [32] H. Kakizakai, K. Yamada, F. Ando, M. Kawaguchi, T. Koyama, S. Kim, T. Moriyama, D. Chiba, and T. Ono, Influence of sloped electric field on magnetic-field-induced domain wall creep in a perpendicularly magnetized Co wire, *Jpn. J. Appl. Phys.* **56**, 050305 (2017).
- [33] A. Vansteenkiste, J. Leliaert, M. Dvornik, M. Helsen, F. Garcia-Sanchez, and B. Van Waeyenberge, The design and verification of MuMax3, *AIP Adv.* **4**, 107133 (2014).
- [34] A. I. Nikitchenko and N. A. Pertsev, Spin-orbit torque control of spin waves in a ferromagnetic waveguide, *Phys. Rev. B* **104**, 134422 (2021).
- [35] S. Subramanian, X. Liu, R. L. Stamps, R. Sooryakumar, and G. A. Prinz, Magnetic anisotropies in body-centered-cubic cobalt films, *Phys. Rev. B* **52**, 10194 (1995).
- [36] H. K. Gweon and S. H. Lim, Relative strength of perpendicular magnetic anisotropy at bottom and top interfaces in Pt/Co/MgO trilayers, *Jpn. J. Appl. Phys.* **57**, 030301 (2018).
- [37] A. I. Nikitchenko and N. A. Pertsev, Generation and routing of nanoscale droplet solitons without compensation of magnetic damping, *Phys. Rev. Mater.* **6**, L101401 (2022).
- [38] A. K. Shukla, M. Goto, X. Xu, K. Nawaoka, J. Suwardy, T. Ohkubo, K. Hono, S. Miwa, and Y. Suzuki, Voltage-controlled magnetic anisotropy in Fe_{1-x}Co_x/Pd/MgO system, *Sci. Rep.* **8**, 10362 (2018).
- [39] N. A. Pertsev, Origin of easy magnetization switching in magnetic tunnel junctions with voltage-controlled interfacial anisotropy, *Sci. Rep.* **3**, 2757 (2013).
- [40] H. Yang, O. Boulle, V. Cros, A. Fert, and M. Chshiev, Controlling Dzyaloshinskii-Moriya interaction via chirality dependent atomic-layer stacking, insulator capping and electric field, *Sci. Rep.* **8**, 12356 (2018).
- [41] W. Zhang, H. Zhong, R. Zang, Y. Zhang, S. Yu, G. Han, G. L. Liu, S. S. Yan, S. Kang, and L. M. Mei, Electrical field enhanced interfacial Dzyaloshinskii-Moriya interaction in MgO/Fe/Pt system, *Appl. Phys. Lett.* **113**, 122406 (2018).
- [42] M. B. Stearns, in *Magnetic Properties of Metals: 3d, 4d and 5d Elements, Alloys and Compounds*, Landolt-Börnstein New Series Group III Vol. 19a (Springer-Verlag, Berlin, 1986).
- [43] O. Boulle, J. Vogel, H. Yang, S. Pizzini, D. de Souza Chaves, A. Locatelli, T. O. Menteş, A. Sala, L. D. Buda-Prejbeanu, O. Klein, M. Belmeguenai, Y. Roussigné, A. Stashkevich, S. M. Chérif, L. Aballe, M. Foerster, M. Chshiev, S. Auffret, I. M. Miron, and G. Gaudin, Room-temperature chiral magnetic skyrmions in ultrathin magnetic nanostructures, *Nat. Nanotechnol.* **11**, 449 (2016).
- [44] B. D. Cullity and C. D. Graham, Magnetic anisotropy, in *Introduction to Magnetic Materials* (Wiley, New York, 2008), Chap. 7, pp. 197–239.
- [45] P. J. Metaxas, J. P. Jamet, A. Mougin, M. Cormier, J. Ferré, V. Baltz, B. Rodmacq, B. Dieny, and R. L. Stamps, Creep and flow regimes of magnetic domain-wall motion in ultrathin Pt/Co/Pt films with perpendicular anisotropy, *Phys. Rev. Lett.* **99**, 217208 (2007).
- [46] A. Aharoni, Demagnetizing factors for rectangular ferromagnetic prisms, *J. Appl. Phys.* **83**, 3432 (1998).
- [47] O. Boulle, S. Rohart, L. D. Buda-Prejbeanu, E. Jué, I. M. Miron, S. Pizzini, J. Vogel, G. Gaudin, and A. Thiaville, Domain wall

- tilting in the presence of the Dzyaloshinskii-Moriya interaction in out-of-plane magnetized magnetic nanotracks, *Phys. Rev. Lett.* **111**, 217203 (2013).
- [48] A. Hubert, *Theorie der Domänenwände in geordneten Medien* (Springer-Verlag, Berlin, 1974).
- [49] E. Martinez, S. Emori, N. Perez, L. Torres, and G. S. D. Beach, Current-driven dynamics of Dzyaloshinskii domain walls in the presence of in-plane fields: Full micromagnetic and one-dimensional analysis, *J. Appl. Phys.* **115**, 213909 (2014).
- [50] J. Torrejon, E. Martinez, and M. Hayashi, Tunable inertia of chiral magnetic domain walls, *Nat. Commun.* **7**, 13533 (2016).
- [51] R. Adler, A study of locking phenomena in oscillators, *Proc. IRE* **34**, 351 (1946).
- [52] N. Kamiya, D. Oshima, S. Iwata, and T. Kato, Perpendicular anisotropy and damping of MBE-grown MgO/Fe/Au(001) and Au/Fe/Au(001) trilayers, *J. Magn. Soc. Jpn.* **45**, 96 (2021).
- [53] A. Koziol-Rachwał, W. Skowroński, T. Ślęzak, D. Wilgocka-Ślęzak, J. Przewoźnik, T. Stobiecki, Q. H. Qin, S. van Dijken, and J. Korecki, Room-temperature perpendicular magnetic anisotropy of MgO/Fe/MgO ultrathin films, *J. Appl. Phys.* **114**, 224307 (2013).
- [54] C. A. F. Vaz, J. A. C. Bland, and G. Lauhoff, Magnetism in ultrathin film structures, *Rep. Prog. Phys.* **71**, 056501 (2008).
- [55] T. Katayama, Y. Suzuki, Y. Nishihara, T. Sugimoto, and M. Hashimoto, Perpendicular magnetic anisotropy in Pt/Fe multilayers, *J. Appl. Phys.* **69**, 5658 (1991).
- [56] J. Ferré, P. J. Metaxas, A. Mougin, J.-P. Jamet, J. Gorchon, and V. Jeudy, Universal magnetic domain wall dynamics in the presence of weak disorder, *C. R. Phys.* **14**, 651 (2013).
- [57] G. S. D. Beach, C. Nistor, C. Knutson, M. Tsoi, and J. L. Erskine, Dynamics of field-driven domain-wall propagation in ferromagnetic nanowires, *Nat. Mater.* **4**, 741 (2005).
- [58] P.-H. Chang, W. Fang, T. Ozaki, and K. D. Belashchenko, Voltage-controlled magnetic anisotropy in antiferromagnetic MgO-capped MnPt films, *Phys. Rev. Mater.* **5**, 054406 (2021).
- [59] F. Chen, Z. Zhang, W. Luo, X. Yang, L. You, and Y. Zhang, Voltage-induced inertial domain wall motion in an antiferromagnetic nanowire, *J. Magn. Magn. Mater.* **511**, 166995 (2020).
- [60] <https://rscf.ru/project/23-12-00251/>